

The silica planar waveguide was fabricated by the sol-gel method using polysiloxane to attain good step coverage and obtain a flat surface. The sol-gel liquid material was spincoated at 1000 rpm onto a substrate where the core had been formed. The sample was baked subsequently at 200°C to solidify the material. The refractive index difference between the core and the planar waveguide ( $n = 1.461$ ) was 0.02. The refractive index difference between the core and the silica underclad was 0.03. The thickness of the planar waveguide was 8  $\mu\text{m}$ .

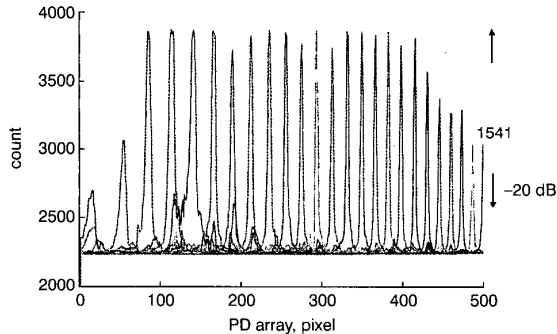


Fig. 2 Measured output from PD array

**Device characteristics:** Fig. 2 shows the output signal from the PD array. The PD array had 512 elements, 25  $\mu\text{m}$  pitch and 500  $\mu\text{m}$  height. The wavelength is varied from 1541 to 1565 nm in 1 nm intervals. The signal sensitivity (PD-output-change/light-input-change) is higher at lower light intensity and tends to saturate at higher light intensity. The device could monitor light from  $-30$  to  $-9$  dBm. The wavelength response was almost flat for the 17 nm range as indicated from the design. The deviation of the peak height is due to the sampling effect of the PD: the peak becomes low when the light spot centre lays in between PD segments. The interpolation software is used in this type of wavelength monitor to cope with the sampling effect. The light with one wavelength was focused across five PD segments.

The secondary peak due to higher-order waveguide modes was lower than  $-20$  dB against the main peak. The focusing spot position of the higher-order mode is different from the spot position of the fundamental mode along the axis perpendicular to PD array direction and spots of both modes can be separated effectively.

It was possible to split lights separated 0.2 nm apart. A spatial dispersion value of  $6 \times 10^5$  was obtained, which is almost an order of magnitude better than equivalent conventional devices. The split in reflectance peak due to polarisation dependence was observed but was  $< 0.1$  nm and indistinguishable for fabrication process yielding low strain. A device with UV written grating based on the same concept of waveguide curve and reflector design was fabricated yielding similar results but with added fabrication procedures making the device not attractive for mass production.

Much higher wavelength resolution and a wider wavelength range of 45 nm can be attained by slightly longer grating (+5 mm) and planar waveguide (+7 mm) structure.

**Conclusions:** A wavelength demultiplexer structure using a channel waveguide grating embedded in a planar waveguide for wavelength monitor has been demonstrated. A segmented waveguide structure was used as a built-in grating. The grating was fabricated simultaneously with the channel waveguide to simplify the fabrication process. The device showed a flat response over 17 nm. It was possible to split lights separated 0.2 nm apart. A spatial dispersion value of  $6 \times 10^5$  was obtained, which is almost an order of magnitude better than equivalent conventional devices.

© IEE 2003

Electronics Letters Online No: 20030531  
DOI: 10.1049/el:20030531

H. Okayama, K. Harase, Y. Uno, H. Ono, H. Takahashi, T. Arakawa, Y. Nishiki and T. Ushikubo (*Optical Components Company,*

18 March 2003

Okai Electric Industry Co. Ltd., 550-1, Higashiasakawa, Hachioji, Tokyo 193-8550, Japan)

E-mail: okayama575@oki.com

## References

- 1 WAGENER, J.L., SRASSER, T.A., PEDRAZZANI, J.R., DEMARCO, J., and DIGIOVANNI, D.J.: 'Fiber grating optical spectrum analyzer tap'. Tech. Dig. ECOC'97, Edinburg, UK, 1997, pp. 65–68
- 2 MADESN, C.K., WAGENER, J., STRASSER, T.A., MILBRODT, M.A., LASKOWSKI, E.J., and DEMARCO, J.: 'Planar waveguide grating optical spectrum analyzer'. Tech. Dig. Integrated Photonics Research, Victoria, Canada, 1998, Paper IMG4
- 3 OKAYAMA, H., and USHIKUBO, T.: 'Wavelength demultiplexer using multi-reflection mirrors positioned along a waveguide'. Tech. Dig. CLEO/Pacific-Rim, Chiba, Japan, 2001, Paper P2-1
- 4 OKAYAMA, H., and TSURUOKA, T.: 'Wavelength demultiplexer using a multi-reflection-mirror waveguide', *Opt. Eng.*, 2002, **41**, (6), pp. 1446–1451

## Distribution of PAR in DMT systems

Hua Yu, Min Chen and Gang Wei

Central limit theorem, modern extreme value theory and the theory that the discrete multitone (DMT) signal converges weakly to a Gaussian random process are employed to derive perfect approximations of peak-to-average envelope power ratio (PAR) distributions of discrete-time and continuous-time DMT signals. Analysis and simulation results show that the PAR problem of DMT is more deteriorative than that of complex-valued OFDM signals.

**Introduction:** Discrete multitone (DMT) and orthogonal frequency division multiplexing (OFDM) have become popular techniques in various high-speed wireless systems owing to the high spectrum efficiency and channel robustness. In general, DMT is denoted as the real-valued OFDM, and widely used in various digital subscriber lines (xDSL) [1]. The principal drawback of DMT and OFDM systems with  $N$  subcarriers is that their peak-to-average envelope power ratio (PAR) may be up to  $N$  times that of corresponding single carrier systems. Recently, there has been a large body of work on approaches to alleviate this undesirable property and on the analysis of the distribution of the PAR [2] in complex-valued OFDM systems. Despite this, the distribution of the PAR in DMT systems has not been reported. In this Letter, we derive a perfect approximation for the PAR of discrete-time DMT signals and an accurate expression for the PAR of continuous-time DMT signals.

The discrete-time DMT signal for with  $N$  subcarriers is represented by

$$s[n] = \frac{2}{\sqrt{2N}} \sum_{k=1}^{N-1} \left( a_k \cos \frac{\pi kn}{N} - b_k \sin \frac{\pi kn}{N} \right) \quad (1)$$

where  $a_k$ s and  $b_k$ s are independent random variables, with zero mean and identical variance, and  $S_k = a_k + jb_k$  are complex symbols from a given PSK or QAM constellation. In (1), the carriers at DC and Nyquist frequency are not used as usual, i.e.  $S_0 = a_0 = b_0 = 0$  [1]. In practice, the signal samples  $\{s[n], n = 0, 1, \dots, 2N-1\}$  are passed through a cutoff frequency  $2\Delta f$  ( $\Delta f$  is the subcarrier spacing) digital-to-analogue (D/A) converter the output of which, ideally, would be closely approximate to the baseband signal waveform

$$s_N(t) = \frac{\sqrt{2}}{\sqrt{N}} \sum_{k=1}^{N-1} \{a_k \cos(2\pi k \Delta f t) - b_k \sin(2\pi k \Delta f t)\}, \quad 0 \leq t \leq T \quad (2)$$

where  $T$  is the symbol period. Since the cyclic prefix cannot introduce any new peaks in the symbol, we assume that  $\Delta f = 1/T$ .

The PAR of continuous-time DMT signals ( $\text{PAR}_c$ ) and the PAR of discrete-time DMT signals ( $\text{PAR}_d$ ) are respectively defined as the ratio of the peak power to the average power of  $s_N(t)$  and the ratio of the maximum to the average of  $s^2[n]$ . In many cases, the continuous-time PAR is approximated using the oversampled discrete-time PAR.

PAR distribution of discrete-time DMT signals: Under the hypothesis for (1), it may be straightforward to show that

$$E\{s[n]\} = 0, \quad D\{s[n]\} = \sigma^2 \quad (3)$$

$$E\{s[m]s[n]\}_{m \neq n} = \begin{cases} 0, & m - n \text{ is odd} \\ -\frac{\sigma^2}{N-1}, & m - n \text{ is even} \end{cases} \quad (4)$$

As  $N \rightarrow \infty$ , (4) becomes

$$E\{s[m]s[n]\}_{m \neq n} \rightarrow 0 \quad (5)$$

Since each of  $s[n]$  is a sum of independent random variables, as  $N$  increases,  $s[n]$  approach Gaussian random variables due to the central limit theorem. So, we can obtain

$$P\left(\frac{s^2[n]}{\sigma^2} \leq r\right) = 2P\left(0 \leq \frac{s[n]}{\sigma} \leq \sqrt{r}\right) \simeq \text{erf}\left(\sqrt{\frac{r}{2}}\right) \quad (6)$$

where  $\text{erf}(t)$  denotes the error function.

Using (5) and (6), the cumulative distribution function of the PAR of discrete-time DMT signals can be approximated as

$$\begin{aligned} P\{PAR_d \leq r\} &\simeq P\left(\frac{s^2[0]}{\sigma^2} \leq r\right) \dots P\left(\frac{s^2[2N-1]}{\sigma^2} \leq r\right) \\ &\simeq \text{erf}^{2N}\left(\sqrt{\frac{r}{2}}\right) \end{aligned} \quad (7)$$

In Fig. 1, the simulation curve of the Nyquist rate sampling is obtained by  $2N$ -point IFFT, and that of the 1024-time oversampling is obtained by SRA developed in [3] with  $K=8$ ,  $M=128$ . It can be seen that the approximation (7) is in good agreement with simulation of the Nyquist rate sampling, which shows the approximation is very accurate in predicting the distribution of the PAR of discrete-time DMT signals. Since the PAR of high enough times oversampled sequences can perfectly approximate to that of continuous-time DMT signals, comparison of the approximation (7) with simulation of the 1024-time oversampling shows that the approximation underestimates the distribution of the PAR of continuous-time DMT signals, and a more accurate expression is needed for predicting the distribution of the PAR of continuous-time DMT signals.

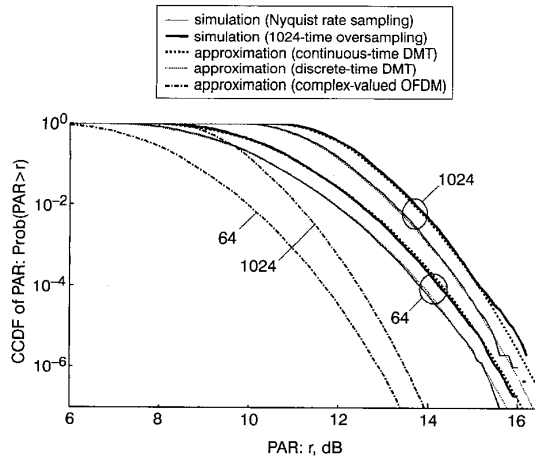


Fig. 1 Comparison of approximations with simulations of PAR in terms of CCDF

$10^7$  and  $10^6$  independent 64-QAM DMT symbols are randomly produced respectively for  $N=64$  and 1024

Distributions of PAR of continuous-time DMT signals: It was established in [2] that a bandlimited OFDM signal and its real part and imaginary part converge weakly to Gaussian random processes. Accordingly, for the DMT signal (2), it is easy to obtain

$$\{s_N(t), 0 \leq t \leq T\} \xrightarrow{D} \{s(t), 0 \leq t \leq T\}, \quad \text{as } N \rightarrow \infty \quad (8)$$

where  $\xrightarrow{D}$  implies convergence in distribution and  $s(t)$  is a zero-mean stationary random process with autocorrelation function

$$E\{s(t)s(t+\tau)\} = \sigma^2 \sin c\left(\frac{2\tau}{\Delta t}\right) \quad (9)$$

where  $\Delta t = T/N$ .

According to the extremal theory [4], let  $\{\xi(t), t \geq 0\}$  be a stationary Gaussian process, with zero mean, unit variance, and autocorrelation function  $r(\tau)$  satisfying

$$\begin{aligned} r(\tau) &= 1 - \frac{\lambda}{2}\tau^2 + o(\tau^2), \quad \text{as } \tau \rightarrow 0 \\ r(\tau) \ln \tau &\rightarrow 0, \quad \text{as } \tau \rightarrow \infty \end{aligned} \quad (10)$$

Then

$$P\{-V_T < m(T) \leq M(T) \leq U_T\} \xrightarrow{T, V_T, U_T \rightarrow \infty} e^{-\eta-\tau} \quad (11)$$

if

$$\begin{aligned} T\mu(U_T) &= \frac{T}{2\pi} \lambda^{1/2} \exp\left(-\frac{U_T^2}{2}\right) \xrightarrow{T, U_T \rightarrow \infty} \tau \\ T\mu(V_T) &= \frac{T}{2\pi} \lambda^{1/2} \exp\left(-\frac{V_T^2}{2}\right) \xrightarrow{T, V_T \rightarrow \infty} \eta \end{aligned} \quad (12)$$

where  $m(T) = \inf\{\xi(t); 0 \leq t \leq T\}$ ,  $M(T) = \sup\{\xi(t); 0 \leq t \leq T\}$ . It is clear that  $\{s(t)/\sigma, 0 \leq t \leq T\}$  is a stationary Gaussian process, with zero mean, unit variance, and autocorrelation function

$$r(\tau) = \frac{E\{s(t)s(t+\tau)\}}{\sigma^2} = \sin c\left(\frac{2\tau}{\Delta t}\right) \quad (13)$$

satisfying conditions stated in (10) with  $\lambda = -r''(0) = (2\pi/\Delta t)^2/3$ . Hence,

$$\begin{aligned} P\left(\max_{0 \leq t \leq T} \left(\frac{s(t)}{\sigma}\right)^2 \leq r\right) \\ = P\left(-\sqrt{r} \leq \min_{0 \leq t \leq T} \frac{s(t)}{\sigma} \leq \max_{0 \leq t \leq T} \frac{s(t)}{\sigma} \leq \sqrt{r}\right) \rightarrow e^{-2\tau} \end{aligned} \quad (14)$$

as  $T, r \rightarrow \infty$ , where

$$\tau \simeq T\mu(\sqrt{r}) = \frac{T}{2\pi} \frac{1}{\sqrt{3}} \frac{2\pi}{\Delta t} \exp\left(-\frac{r}{2}\right) = \frac{N}{\sqrt{3}} \exp\left(-\frac{r}{2}\right) \quad (15)$$

as  $N, r \rightarrow \infty$ . Therefore, the cumulative distribution function of the PAR of continuous-time DMT signals can be approximated as

$$\begin{aligned} P\{PAR_c \leq r\} &= P\left\{\max_{0 \leq t \leq T} \frac{s_N^2(t)}{\sigma^2} \leq r\right\} \\ &\simeq \exp\left\{-\frac{2N}{\sqrt{3}} e^{-r/2}\right\} \end{aligned} \quad (16)$$

when  $N$  and  $r$  are large enough.

From Fig. 1, it can be seen that there is close agreement of the proposed expression (16) with the simulated distribution of the PAR for a number of subcarriers as small as 64. Comparison of (16) with the approximation for continuous-time complex-valued OFDM signals [2] is also shown in Fig. 1. It shows that the PAR problem of DMT is more deteriorative than that of complex-valued OFDM signals. For example, at the probability of  $10^{-4}$ , the PAR of DMT signals is 2.5 dB larger than that of OFDM signals. Therefore, we should pay more attention on the PAR problem in DMT systems.

Conclusion: Perfect approximations of the PAR of discrete-time DMT signals and the PAR of continuous-time DMT signals are derived. Analysis and simulation results show that the PAR problem of DMT is more deteriorative than that of complex-valued OFDM signals.

Acknowledgments: The support of the NSF China (Grant 60072048) and the Doctoral Program Fund of the Educational Ministry of China (Grant 20010561007) are gratefully acknowledged.

Hua Yu, Min Chen and Gang Wei (School of Electronic & Information Engineering, South China University of Technology, Guangzhou, 510640, People's Republic of China)

E-mail: yuhuahao@163.com

## References

- 1 ITU-T: 'Asymmetric digital subscriber line (ADSL) transceivers'. ITU Standard, R. G. 992.1, June 1999
- 2 WEI, S., GOECKEL, D.L., and KELLY, P.E.: 'A modern extreme value theory approach to calculating the distribution of the peak-to-average power ratio in OFDM Systems'. IEEE Int. Conf. on Communications, New York, NC, USA, 2002, Vol. 3, pp. 1686-1690
- 3 YU, H., LIN, Y., and WEI, G.: 'High precision and fast computation of the PAR of continuous-time OFDM and DMT signals', *IEEE Commun. Lett.*, (accepted)
- 4 BERMAN, S.M.: 'Asymptotic independence of numbers of high and low level crossings of stationary Gaussian processes', *Ann. Math. Stat.*, 1971, 42, pp. 927-945

## Dynamic bandwidth sharing for handoff traffic in multimedia mobile cellular networks

Qian Huang, Sammy Chan and King-Tim Ko

An efficient handoff control scheme using dynamic bandwidth sharing in multimedia mobile cellular networks is presented. The numerical results show that compared to the commonly used bandwidth reservation based handoff control scheme, higher bandwidth utilisation is achieved in the proposed scheme under different traffic loading distributions, while lower call dropping probabilities are also maintained.

**Introduction:** In the past, various handoff control schemes based on bandwidth reservation have been proposed for multimedia mobile cellular networks [1-3]. The basic idea of these schemes is that a dynamically adjustable size of resources is reserved in neighbouring cells exclusively for handoff calls of real-time traffic, in order to reduce the probabilities of handoff dropping caused by insufficient bandwidth available in the target cell. However, this kind of scheme causes low bandwidth utilisation in multimedia scenarios owing to the bandwidth exclusively reserved for handoff calls of real-time traffic not being allowed to be used by any type of new calls and handoff calls of non-real-time traffic, even when this reserved bandwidth is not being used [3].

In this Letter, we propose an enhanced handoff control scheme allowing dynamic bandwidth sharing between different types of traffic for improving bandwidth utilisation in scenarios of multiple traffic classes. The distinct feature of the proposed scheme is that even if there is not sufficient free bandwidth and reserved bandwidth in the target cell, handoff calls of real-time traffic can be admitted by borrowing the necessary bandwidth from existing non-real-time connections with allocated maximal bandwidth; for handoff calls of non-real-time traffic, when the free bandwidth in the target cell is exhausted, the bandwidth reserved for but not being used by real-time handoff calls (defined as *overbooked bandwidth*) in the cell can be dynamically shared by these handoff calls. In this way, a higher bandwidth utilisation and lower call dropping probabilities can be achieved.

**Scheme description:** We consider a cellular mobile network which provides two typical types of services: class 1 service provides QoS guarantee and is therefore suitable for voice or video services; class 2 service is a best-effort service but with a minimal bandwidth requirement, which is suitable for data traffic such as file transfer. The required bandwidth of class 1 calls is  $B_1$  and it is fixed throughout the call duration. Conversely, the required bandwidth of class 2 calls is

flexible. Their minimum required bandwidth is  $B_{2m}$ , and if there is bandwidth available, they are allocated with their maximum required bandwidth  $B_2$ , where  $B_2 > B_1$ . In the following description, the *free bandwidth* of a cell is defined as the bandwidth which has not been allocated to or reserved for any calls.

Our proposed handoff control scheme operates as follows. First, for class 1 handoff calls, their requested bandwidth  $B_1$  will be reserved in the immediate neighbouring cells for the next possible handoff using the simple bandwidth reservation algorithm similar to that of [2], i.e. reserving bandwidth for possible real-time handoff calls based on the estimated movement probabilities of a call into its neighbouring cell. Note that how to predict user mobility pattern and movement probability is beyond the scope of this Letter (detailed research on this issue can be found in [4]). (In our simulations, it is assumed that the movement probability of a call from the current cell to the next adjacent cell is known.) Since best-effort traffic can tolerate longer transmission latency, the dropped packets due to handoff failure can be recovered by retransmission. Therefore, no bandwidth is reserved in the neighbouring cells for possible handoff use in class 2 traffic. Secondly, the proposed scheme decides whether to accept a handoff call based on dynamic bandwidth sharing between the two different classes of handoff calls. When a class 1 call handoffs to a neighbouring cell, even if there is not sufficient reserved bandwidth in that cell, the network would accept it by borrowing the necessary bandwidth from existing class 2 connections with allocated maximal bandwidth  $B_2$ . To improve bandwidth utilisation and minimise the handoff dropping probability for class 2 calls, our proposed scheme allows a class 2 handoff call to be admitted by temporarily borrowing the *overbooked bandwidth* from the future incoming class 1 calls, when the free bandwidth in the target cell cannot support the minimal bandwidth requirement  $B_{2m}$ . However, when a class 1 handoff call arrives, the borrowed bandwidth  $B_1$  by the class 2 handoff call will be recalled to accept this class 1 handoff call, if there is no free bandwidth and reserved bandwidth in the cell available for this class 1 call.

**Performance comparisons:** In this Section, we choose the typical bandwidth reservation based handoff control scheme similar to that of [2] for performance comparisons with our proposed scheme by simulations using OPNET packages [5]. We define the simple bandwidth reservation based scheme as scheme A, which operates as follows. It reserves bandwidth for possible class 1 handoff calls based on the estimated movement probabilities of a call into its neighbouring cell, and accepts class 2 handoff calls with best-effort. If both the free bandwidth and reserved bandwidth in the target cell are exhausted, the arriving class 1 handoff calls will be dropped. For class 2 handoff calls, they are dropped as long as the free bandwidth in the target cell is less than the minimal bandwidth  $B_{2m}$ .

The parameters used in our simulations are as follows. The total bandwidth of the wireless link is set to 2 M bits/s, and the maximal reserved bandwidth in each cell equals to 20% of the total bandwidth. The constant bandwidth of class 1 calls  $B_1$  is set to 64 k bits/s, the peak rate of class 2 calls  $B_2$  is set to 128 k bits/s and the minimal bandwidth  $B_{2m} = 64$  k bits/s. New call arrivals of both traffic classes are assumed to follow a Poisson process with an average rate  $\lambda_c$  (its value is variable), where  $c = 1, 2$ . The call holding time and call dwelling time of both traffic classes are assumed to be exponentially distributed with mean equal to  $1/\mu_1 = 1/\mu_2 = 200$  s and  $1/\eta_1 = 1/\eta_2 = 100$  s, respectively.

In the following two Sections, we compare the call dropping probability and bandwidth utilisation of the proposed scheme with scheme A under different combinations of offered load. We define  $Q$  as the percentage of class 1 traffic in the offered load in a cell and  $Q = \lambda_1 B_1 / (\lambda_2 B_2 + \lambda_1 B_1)$ , since  $1/\eta_1 = 1/\eta_2$  is set here.  $Q = 20, 50, 67\%$  are chosen in our simulations, which correspond to three cases of traffic load distributions in a cell.

**Call dropping probabilities:** Fig. 1 shows that our proposed scheme achieves lower dropping probabilities of class 1 calls than scheme A under different  $Q$ , since more class 1 handoff calls can be accepted in our scheme by dynamically borrowing bandwidth from existing class 2 connections with peak rate  $B_2$ , when both the free bandwidth and reserved bandwidth in the target cell are exhausted. Fig. 2 shows that the dropping probabilities of class 2 calls in the proposed scheme are also lower than that of scheme A under different  $Q$ . This is because